UNIVERSITY OF BIRMINGHAM
University of Birmingham Research at Birmingham

The role of powder atomisation route on the microstructure and mechanical properties of hot isostatically pressed Inconel 625

Sergi, Alessandro; Khan, Raja H.U.; Attallah, Moataz M.

DOI:
10.1016/j.msea.2021.140950

License:
Other (please provide link to licence statement

Document Version
Peer reviewed version

Citation for published version (Harvard):
Sergi, A, Khan, RHU & Attallah, MM 2021, 'The role of powder atomisation route on the microstructure and mechanical properties of hot isostatically pressed Inconel 625', *Materials Science and Engineering A*, vol. 808, 140950. https://doi.org/10.1016/j.msea.2021.140950

Link to publication on Research at Birmingham portal

General rights
Unless a licence is specified above, all rights (including copyright and moral rights) in this document are retained by the authors and/or the copyright holders. The express permission of the copyright holder must be obtained for any use of this material other than for purposes permitted by law.

•Users may freely distribute the URL that is used to identify this publication.
•Users may download and/or print one copy of the publication from the University of Birmingham research portal for the purpose of private study or non-commercial research.
•User may use extracts from the document in line with the concept of 'fair dealing' under the Copyright, Designs and Patents Act 1988 (?)
•Users may not further distribute the material nor use it for the purposes of commercial gain.

Where a licence is displayed above, please note the terms and conditions of the licence govern your use of this document.

When citing, please reference the published version.

Take down policy
While the University of Birmingham exercises care and attention in making items available there are rare occasions when an item has been uploaded in error or has been deemed to be commercially or otherwise sensitive.

If you believe that this is the case for this document, please contact UBIRA@lists.bham.ac.uk providing details and we will remove access to the work immediately and investigate.

Download date: 25. Apr. 2024

The Role of Powder Atomisation Route on the Microstructure and Mechanical Properties of Hot Isostatically Pressed Inconel 625

Alessandro Sergi[1, 2], Raja H. U. Khan[3], Moataz M. Attallah*[1]

[1] IRC in Materials Processing, School of Metallurgy and Materials, The University of Birmingham, Birmingham, B15 2TT, UK

[2] National Structural Integrity Research Centre (NSIRC), Cambridge, CB21 6AL, UK

[3] TWI Ltd, Cambridge, CB21 6AL, UK

* Corresponding author: m.m.attallah@bham.ac.uk

Abstract

The powder's characteristics and its purity can greatly influence the properties of nickel (Ni)-base superalloys parts produced by near net-shape powder metallurgy hot isostatic pressing (NNS PM HIP) manufacturing process. In this study, Inconel 625 (IN625) powders produced using four different atomisation routes, argon, nitrogen, plasma and water atomisation (AGA, NGA, PA, WA, respectively) were investigated. The first section of this study is focused on the determination of powder characteristics which includes chemical composition, particle size distribution (PSD), tap density and powder's cross-section analysis, whereas the second section is about hot isostatic pressing (HIPping) of the four powder types and to assess the impact of the powder characteristics on the microstructure-property development after HIPping. To gain an understanding of the surface chemistry of the powders, X-ray photoelectron spectroscopy (XPS) analysis were carried out on the surface of the four powders. The latter analysis highlighted fundamental differences on the powder's surface, especially the differences in the surface and near-surface distribution of the alloying elements i.e. C, O, Cr, Mo and Nb present in the alloy chemistry. The micrographs of the four IN625 hot isostatically pressed (HIPped) powders revealed a fully dense microstructure with the presence of prior particle boundaries (PPBs). The atomisation route greatly impacted the nature

and amount of PPBs, as well as on the fractions and sizes of oxides, carbides, oxycarbides and oxycarbonitrides precipitates. WA showed the most severe presence of PPBs, followed by NGA, AGA and lastly PA. The powder quality has a greater impact on the mechanical properties of as-HIPped materials, especially on ductility. Overall, PA HIPped IN625 possessed the optimum balance between tensile strength, ductility and Charpy impact properties once compared to the others and match the properties to wrought IN625 material.

Keywords: Ni-base Superalloys; Powder Metallurgy Hot Isostatic Pressing; X-ray photoelectron spectroscopy; Microstructure; Mechanical properties

1. Introduction

Near netshape powder metallurgy hot isostatic pressing (NNS PM HIP) is an advanced manufacturing technique capable of producing near to net-shape complex engineering parts with excellent isotropic mechanical properties and improved buy-to-fly ratios. HIPping has been successfully performed on a wide range of powder materials, including Ni-base superalloys [1] which has shown different challenges. One of the challenge is the presence of unwanted and detrimental precipitates at prior particle boundaries (PPBs) in the microstructure of HIPped Ni-base superalloys. The particles manifested inside PPBs can be of different types, including oxides, carbides, and oxycarbonitrides. The presence of PPBs in the HIPped material can influence; the powder consolidation and the resulted mechanical properties i.e. tensile strength, ductility, fatigue life and fracture toughness. PPBs reduce the inter particle bonding, thus dramatically reduce the elongation-to-failure and fracture toughness [2] [3].

To mitigate this undesirable preferential precipitation process, it must need to be understood how these particles are generated and how the HIPping parameters influence their formation mechanisms. The generation of PPBs during HIPping has its origin during the atomisation process, where a thin oxide layer is generated [4]. This is supported by several studies, where the presence of

a thin oxide layer at the surface of the powder has been detected via XPS [5], [6], [7]. Gao *et al.* [8], showed a high concentration of oxygen and elemental segregation on the surface of the powder of FGH96 Ni-based superalloy, which then creates a thin oxide layer during the HIPping process. This layer is composed of TiO_2, Cr_2O_3 and ZrO_2 [8]. Since these oxides are stable at considerably higher temperatures, they will not dissolve during HIPping and will still be present at the PPBs after the consolidation has taken place. Many authors have claimed that the oxides present at the particle boundaries act as preferential sites for the formation of carbides at PPBs, leading to deteriorate mechanical properties [3], [9], [10]. Many attempts have been proposed to eliminate or reduce the presence of oxycarbides at PPBs, with is one of the most used approaches relying on post-HIP heat treatment to dissolve the precipitates [11] [12]. However, these attempts were not always successful due to the high dissolution temperatures of oxides and carbides, which often exceed the solvus temperatures of the alloy [13] and generate excessive grain growth which impairs the microstructure and ultimately the mechanical properties. Among all the proposed methods, the most agreed upon practice for reducing the amount of PPBs is to improve the quality of the powders, as powders with lower O levels result in a lower presence of PPBs, thus a drastic improvement in the mechanical properties [3].

In this study, the impact of the powder's characteristics on the microstructure and room temperature mechanical properties of HIPped IN625 were evaluated. IN625 Ni-based superalloy was selected for this investigation to assess the effect of the powder's characteristics on the HIP response of the material for several reasons. Firstly, IN625 is widely used in the marine, aerospace and nuclear sectors thanks to the excellent corrosion resistance and high temperature strength. This study can unveal opportunities for different applications for powder HIPped IN625 depending on the performance and component requirements (including the cost). Secondly, IN625 is susceptible to the formation of PPBs, mainly due to the presence of Cr, Nb, and Mo, allowing for the influence of the powder characteristics and atomisation route on the PPBs formation to be rationalised. Thirdly, IN625 is mainly a solid solution strengthened alloy with a limited or no formation of γ'' in the as-

HIPped conditions. Thus, it is relatively easier to elucidate the mechanical performance of the different powder batches, having less microstrucural variables to consider. This also makes it easier to understand the influence of the interstitials such as O, C and N on PPBs formation and mechanical properties, due to the relatively simpler microstructure if compared with other Ni-base superalloys. Finally, since there is a substantial difference in price among the four IN625 powders, the use of lower quality/lower cost powders (NGA or WA), can drastically reduce the manufacturing costs and can be considered for low value compenets where a superior mechanical performance is not required.

2. Materials and Experimental Methods

In this study, HIPping was performed on four different IN625 powders – AGA (15-45µm), NGA (15-150µm), PA (0-150µm) and WA (15-150µm). The powders' morphology, particles cross-section microstructure, chemical composition, surface atomic chemical composition and physical properties (flowability, densities and particle size distribution (PSD)) were assessed. Chemical analysis of the four IN625 powders were performed by AMG Analytical Services, Sheffield. The inductively coupled plasma optical emission spectroscopy (ICP OES) technique was employed to determine the major alloying including any impurity elements, such as Cr, Mo, Nb, W, Cu, Ni, Co, Fe, Mn, V, Ti, Sn, Al, Si, P, Ta and B (lower limit <0.02%) [14]. C and S were determined by LECO thermal infrared using combustion in oxygen, whereas O, N and H gases were determined by LECO inert gas fusion using infrared and thermal conductivity detection [15], [16]. XPS was performed using a monochromatic X-ray $K\alpha_1$ source. The C1s carbon binding energy (B.E.) of 284.8eV was used for calibration to consider the charging effects. XPS depth profiles were obtained through argon ion beam etching using 1000eV. The PSDs of the four powders were measured at TWI Ltd. using a Malvern Matersizer 3000 laser diffractometer. Flowability of all four powders was measured using Hall flowmeter as per ASTM B213-17. The apparent and tap density measurements were performed according to ASTM 212-17 and ASTM B527-15 standards,

respectively. After characterisation, the four powders were encapsulated in TIG welded mild steel canisters (Ø50mm x 185mm) with 2mm wall thickness. All the canister were leak tested using helium leak detector before loading/filling the powders. The filling procedure was performed in a controlled environment inside an argon filled glovebox, after which the canisters were de-gassed for 48 hours and hot sealed. The four canisters were then HIPped using the EPSI HIP, available at the University of Birmingham (UoB). The HIPping parameters used were; a temperature of 1160°C, pressure of 120MPa and dwell time of four hours with heating rate of 5°C/min and cooling rate of 10°C/min (Figure 1). The above mentioned parameters are commonly used parameters during HIPping IN625 powder [17]. The HIPped samples were extracted using electric discharge machining (EDM) cutting, mounted in conductive bakelite and grounded/polished using standard metallographic procedures for Ni-superalloys. The HIPped IN625 material's microstructure was then analysed using a Hitachi TM3000 Scanning Electron Microscope (SEM) in backscattered electrons (BSE) mode. Electron-backscattered diffraction (EBSD) analysis was also performed on the HIPped microstructures using a Philips XL-30 SEM, using a step size of 1μm, with the results post-processed using HKL Channel 5 software. Vickers microhardness measurements were performed using a semi-automatic Buehler microhardness tester at ten different locations for each sample, according to ASTM E384 – 17, using a load of 500gf and a holding time of 10s. Room temperature tensile tests were performed as per ASTM E8/E8M-16a standards on HIPped IN625 samples. Whereas, room temperature Charpy impact tests were performed on HIPped IN625 samples measuring 10mm x 10mm x 55mm, with a 2mm Charpy V-notch as per ASTM E23-16b standards.

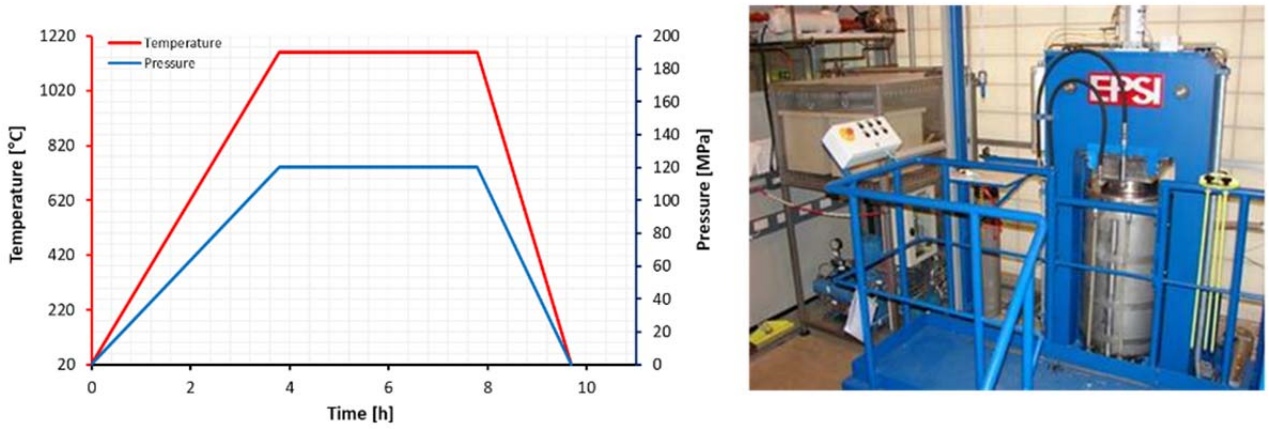

Figure 1 Schematic of the HIP cycle (left); EPSI HIP at UoB (right).

Two different heat treatments (HT) were performed on the as-HIPped IN625 to further improve the microstructural homogeneity by dissolving any detrimental phases, and subsequently assessing their impact on the mechanical properties. The first heat treatment (HT1) consists of the following steps (Figure 2):

- Solution heat treatment (SHT) at 1180°C for one hour, followed by Ar fast cooling according to AMS 2774E [18].
- First aging precipitation treatment at 720°C for 8.5 hours to precipitate the limited quantity of gamma double prime (γ′′) [Ni_3Nb] phase in this alloy, followed by cooling to 620°C at 50°C/h.
- Second aging precipitation treatment at 620°C for 8.5 hours, followed by furnace cooling to room temperature.

The purpose of using high SHT temperature during HT1 was to dissolve any unwanted detrimental phases which might have been precipitated/formed during the HIP process, such as Laves $[Fe, Cr]_2(Nb, Mo)$ (dissolution temperature in the order of 1100°C [19] and delta (δ) [Ni_3Nb] with a dissolution temperature of around 1025°C [20]. Whereas, double aging treatments are similar as presented in literature [21], [22] and AMS 2774E. Furthermore, HT1 promotes the grain growth past the PPBs and precipitation of γ′′.

The second heat treatment (HT2) was performed only on HIPped PA IN625 material with similar aging steps, while lowering the solution temperature to 1050°C (Figure 2):

The HT2 cycle consisted of the following steps:

- SHT at 1050°C for one hour under vacuum, followed by Ar fast cooling according to AMS 2774E [18].
- First aging precipitation treatment at 720°C for 8.5 hours, followed by cooling to 620°C at 50°C/h.
- Second aging precipitation treatment at 620°C for 8.5 hours, followed by furnace cooling to room temperature.

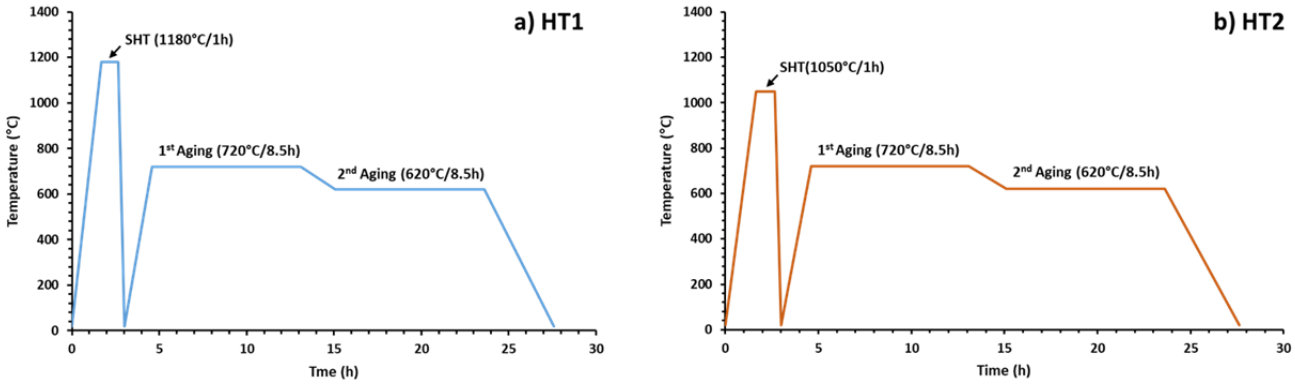

Figure 2 Schematic of post-HIP heat treatment, (a) HT1 and (b) HT2.

3. Results and Discussion

3.1. Powder characterisation: chemical composition, size, morphology, and flowability

A considerable difference exists within the chemical composition of the four different powders. Table 1 shows the differences in the oxygen (O) levels between the four atomisation routes, with WA powders having an O level of 7100ppm, far above the standard level for IN625 [23]. Although O level in NGA powder is lower than WA however it is still above the standard allowable range. The O level in PA and AGA powders are comparatively low and within the standard. Another factor affecting the formation of PPBs is represented by the carbon and nitrogen content. WA and NGA show lower levels of carbon compared to AGA and PA, while NGA showed higher levels of

nitrogen, above the specifications. Few other alloying elements such as Cr, Mo, Fe and Nb for all the four powders are within the typical allowable range for IN625. Additionally, since WA and NGA were melted and atomised in an ambient atmosphere, Al and Ti were not included during the atomisation process. This is due to the reactive nature of these elements, as they have the tendency to form stable oxides. The N content is relatively high in NGA powder which is due to atomisation nitrogen gas, as expected, and this can promote the formation of oxycarbonitrides [24]. The Si content was higher than the standard range in NGA and WA, since Si is added to increase the melt flow during the atomisation process. Furthermore, Mo and Fe contents were higher in AGA, which will provide higher levels of solid solution strengthening compared to the other powders. Although, the amount of Ti and Al in PA and AGA powders is within the allowable range however is higher than the WA and NGA powders, which could potentially promote the precipitation hardening during the aging treatment.

Table 1 Chemical composition of the four IN625 powders (wt.%).

Elements	C	O	N	Cr	Fe	Cu	Mn	Mo	Ni	P	S	Si	Nb	Al	Ti	Co
Required [25]	<0.10	<0.02	<0.02	20.0-23.0	≤5.0	<0.50	<0.50	8.0-10.0	bal ≥58	<0.015	<0.015	<0.50	3.15-4.15	0.1-0.4	0.1-0.4	≤1.0
AGA (15-45µm)	0.02	0.01	0.009	20.8	4.20	0.02	0.02	9.10	61.58	<0.005	<0.005	0.08	3.64	0.21	0.21	0.1
NGA (15-150µm)	0.009	0.06	0.07	20.32	3.12	0.03	0.56	8.48	63.28	0.007	0.004	0.79	3.18	<0.03	<0.02	0.02
PA (0-150µm)	0.03	0.01	0.009	21.47	1.37	0.01	0.06	8.71	64.32	0.002	<0.001	0.06	3.59	0.23	0.11	0.02
WA (15-150µm)	0.004	0.71	0.02	21.29	3.32	0.03	0.42	8.41	61.64	0.006	0.005	0.71	3.35	<0.02	<0.02	<0.02

The powder morphology study has identified differences between the four IN625 powders. AGA had a nearly spherical shape, with the presence of satellites and irregularly-shaped powder particles. NGA had a nearly spherical shape and a more regular morphology. As expected, PA powders had the best spherical shape once compare to the rest of the powders used, with a bi-modal PSD. WA powders had a typically irregular shape, as a result of the WA atomisation process (Figure 3), this was also observed in the work of A. Mostafaei *et al.* [26]. The oxidation of the melt during WA increases the surface tension of the droplet, restricting the likelihood of particle

spheroidisation [27]. Furthermore, the surface of WA powders appear to be inhomogeneous with micro-segregation of Ni, Nb and Mo, as shown in the Energy-dispersive X-ray spectroscopy (EDS) maps (Figure 4). The cross-section of the powders reveal little-to-no porosity in NGA and PA, while AGA has minimal entrapped porosity arising from the atomisation route (Figure 5). The presence of porosity is attributed to argon being a non-soluble gas, thus it will remain entrapped inside the molten droplets during the atomisation[27]. The SEM micrographs of Figure 5 reveal the influence of the cooling rate on the powder cell size. In particular, WA process has the highest cooling rate; this is confirmed by the presence of a small cell size. In AGA, the small particle size promotes high cooling rates during the atomisation process and consequently a small cell size is present. On the other hand, PA process possess relatively lower cooling rates [27], thus a bigger cell size can be observed in Figure 5. Furthermore, the backscattered micrographs (Figure 5) also show Mo and Nb enriched micro-segregation inside the individual particles [28].

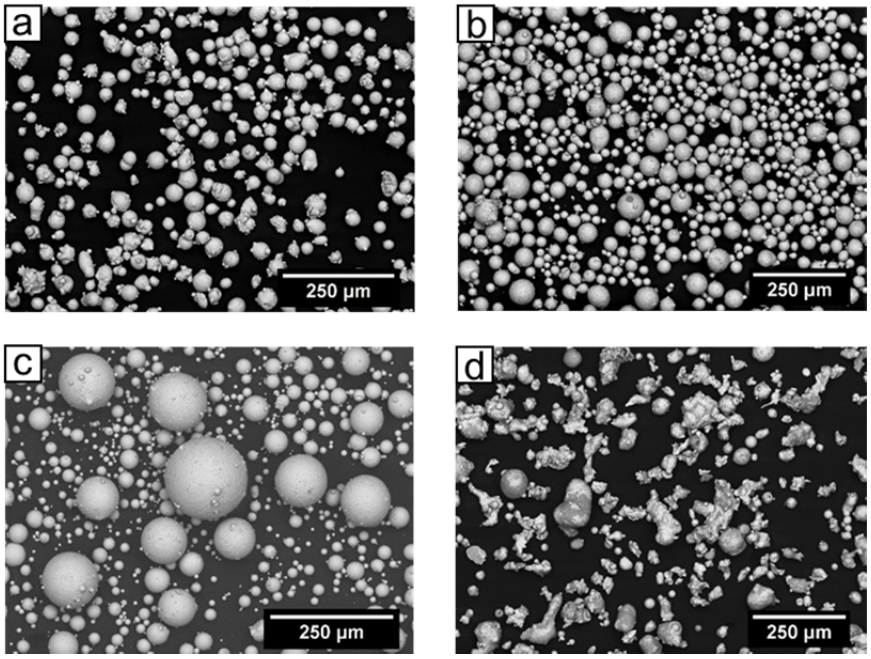

Figure 3 Backscattered SEM micrographs of IN625 powders: (a) AGA (15-45µm); (b) NGA (15-150µm); (c) PA (0-150µm); (d) WA (15-150µm).

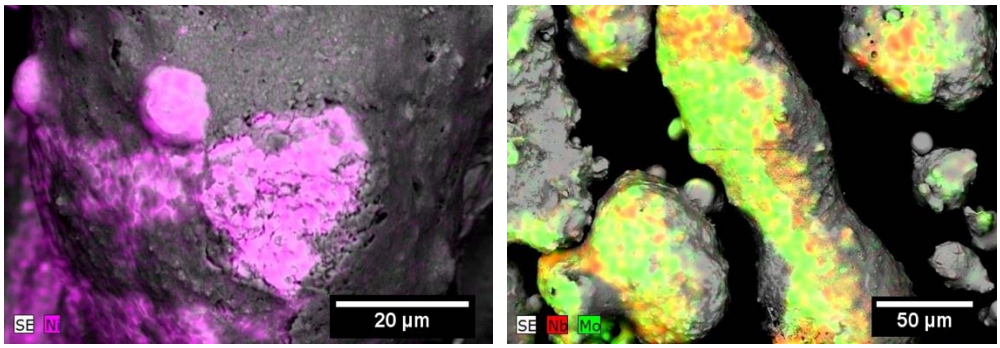

Figure 4 EDS maps on the surface of WA powders, showing segregation of Ni, Nb and Mo on the surface.

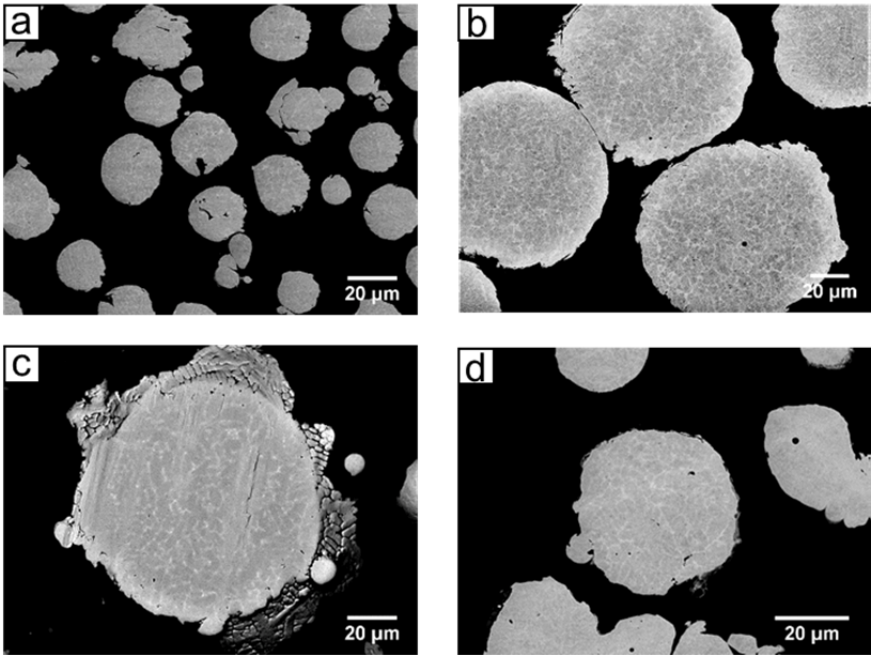

Figure 5 Backscattered SEM micrographs of IN625 powder's cross-section: (a) AGA; (b) NGA; (c) PA; (d) WA.

Differences in the four powders can be seen in terms of estimated PSD values. WA, NGA and PA have a wider size range, while AGA has a narrower size range, with a D_{90} of just 40µm (Table 2). The values of $D_{10,}$ D_{50} and D_{90} for AGA IN625 are comparable to the results proposed by Pleass *et al.* [29]. Tap density is directly linked with the powder's particle size range, PSD and morphology; PA powder has the highest packing density, due to the combination of its spherical morphology, bi-modal particle size distribution and wider particle size range (Figure 6). NGA has a high packing density due to its spherical morphology, as well as the wider PSD range and the absence of satellites. Despite NGA, WA and PA having similar particle size range, each with a

wider range distribution, WA powders have a lower packing density, due to the highly irregular morphology of the powder. Lastly, AGA has a packing density of 61%, higher if compared to the work of Pleass *et al.*, [29]. The lower packing density of AGA powder if compared to NGA and PA is a consequence of the narrow powder particle size range and PSD. Differences in flowability can be also observed. Among the four powders, PA powders show the best flow rate thanks to its highly regular shape, while WA showed a poor flow rate due to the irregular shape of the powders.

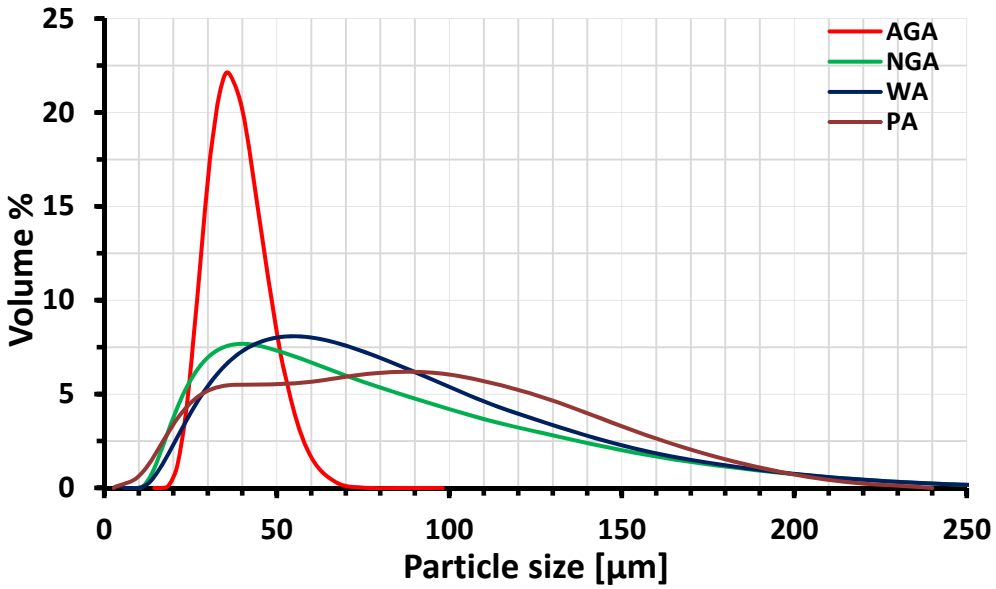

Figure 6 PSD of IN625 powders.

Table 2 Physical Properties of IN625 powders.

Powder Type	Tap Density (g/cm3)	Packing Density (%)	Flow rate (s/50g)	PSD (µm)		
				D10	D50	D90
AGA IN625	5.12	60.66	14.32	20	29	40
NGA IN625	5.63	66.71	13.42	23	49	121
PA IN625	6.01	71.20	12.73	17	49	122
WA IN625	4.45	52.72	21.62	27	58	126

3.2. Surface characterisation of the powders using XPS

Chemical analysis may not be enough to describe the response of certain powders to HIPping and to determine the root cause of the formation of PPBs. The study of surface composition of the powders

is necessary to understand whether an oxide surface layer exists, and which elements are most prone to micro-segregation. For this reason, XPS analyses have been performed on the four different powders. XPS depth surface analysis focused on the major elements influencing the formation of PPBs, such as Nb, Mo, Cr, C and O, with their depth profiles reported in Figure 7. The first noteworthy result is represented by the high concentration of O on the surface of each powder. However, a distinction must be made: AGA and PA have a lower amount of O on their surfaces, followed in order by NGA and WA. Although C content in all the powders is below the allowable limit, it still can play and important role in the formation of PPBs in HIPped IN625. C-content is higher in AGA, PA and NGA surfaces, while WA powder has the lowest amount of C on the surface, as well as on the bulk (Table 1). The distribution of Nb suggests that for AGA, NGA and WA there is a higher concentration on the powder's surface, or in its proximity, this can be an important factor, which influences the formation of NbC at PPBs. The distribution of Nb in PA follows a flatter trend with no obvious differences in concentration along the depth of the powder. The presence of Cr in AGA, NGA and PA is around 20wt.%, which is well within the required limit (Table 1), while in WA there is a stronger presence of Cr (around 30wt.%) at the powder surface at the expense of Ni. This suggests that higher O levels on the surface promotes the diffusion of Cr to the outer surface of powder with the generation of Cr_2O_3. This reaction can occur during atomisation, despite the high cooling rates, due to the high diffusion coefficient of Cr in Ni of $1.1x10^{-4}m^2/sec$, the highest among all the alloying elements present in IN625 [30].

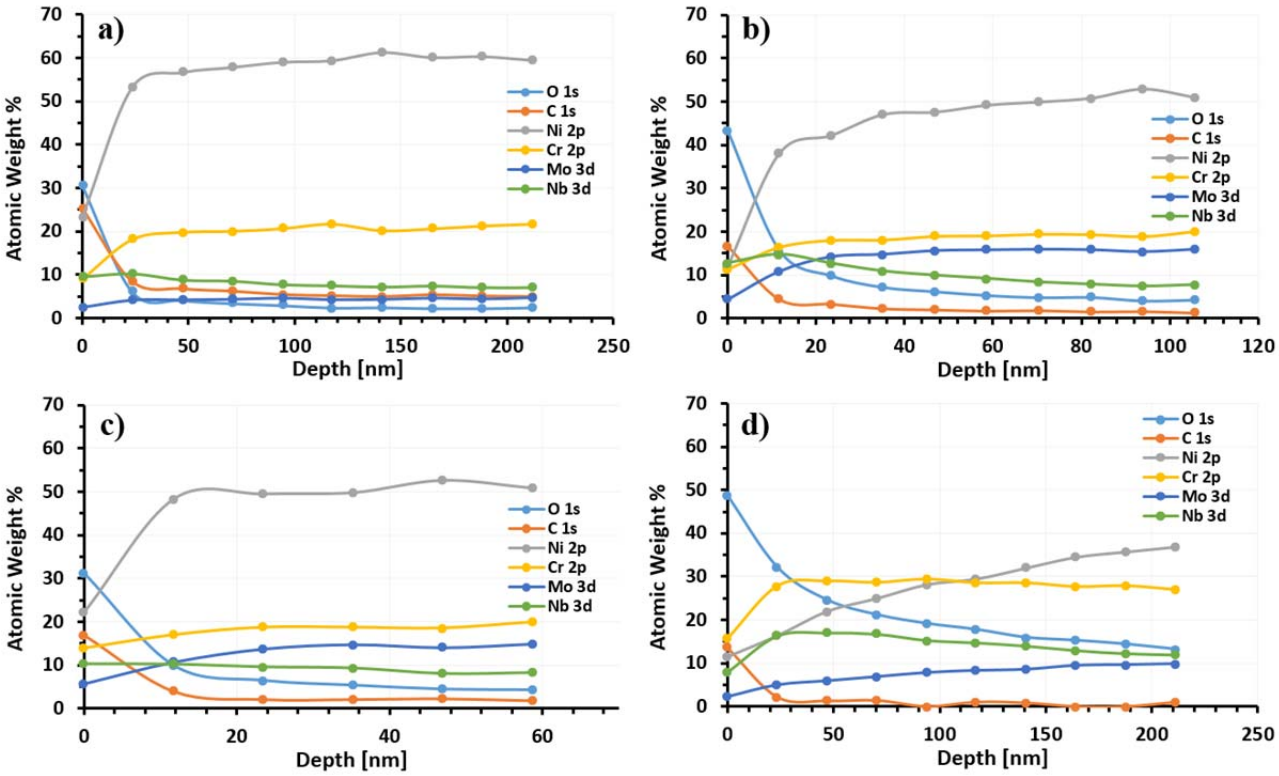

Figure 7 XPS depth profiles for: (a) AGA; (b) NGA; (c) PA; (d) WA IN625 powders.

A more detailed analysis of the surface chemistry of powders, as well as at 70nm etch depths for all powders, and up to 210nm for WA, is reported here in Figure 8**Error! Reference source not found.**. The most dominant peak on the surface is represented by O1s, as well as a strong peak of C1s. Their intensity decreases at 70nm depth in AGA, NGA and PA, while for WA, the O1s peak is still present up to and beyond 210nm depth, meaning a thicker oxide layer is formed during WA. The presence of Ti on the surface of AGA and PA powders is represented, which is noteworthy as Ti can lead to the formation of TiO_2 and TiC at PPBs during the consolidation process [31]. No presence of Ti was observed on the surface of NGA and WA powders. Another important difference is represented by the presence of Si on the surface of NGA and WA.

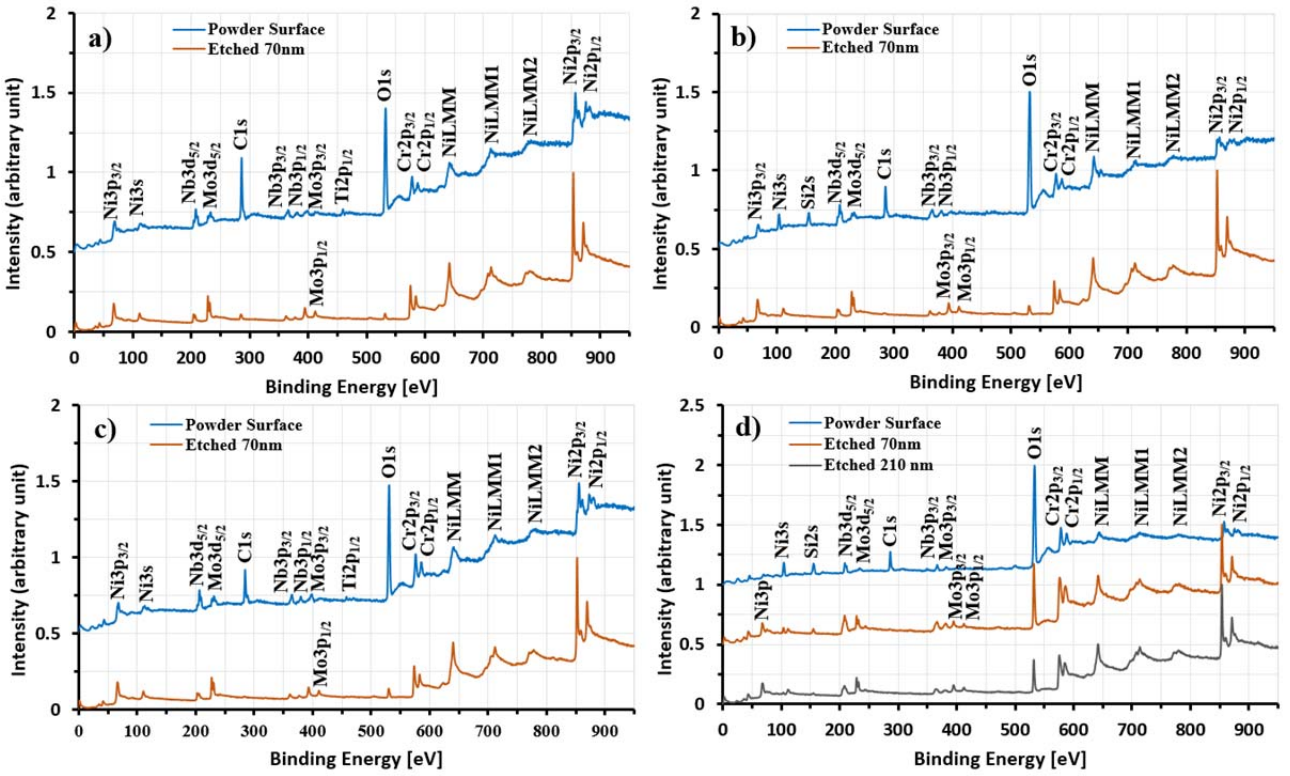

Figure 8 XPS spectra on the surface of the powder and at 70nm from the surface for: (a) AGA; (b) NGA; (c) PA; (d) WA IN625 powders.

Higher resolution XPS performed on the distribution of Nb on the surface shows the presence of different oxidation states, including NbO_2 and Nb_2O_5, for all powders [32]. WA shows a weaker presence of Nb on the surface of the powder with the absence of carbide peak, suggesting that no NbC is observed on the surface of the WA powder, while for AGA, NGA and PA, NbC is observed, in line with other studies [24], [33]. The absence of NbC on the surface of WA powders can be attributed to the combination of higher cooling rates during atomisation, together with negligible concentration of C in pre-alloyed powders.

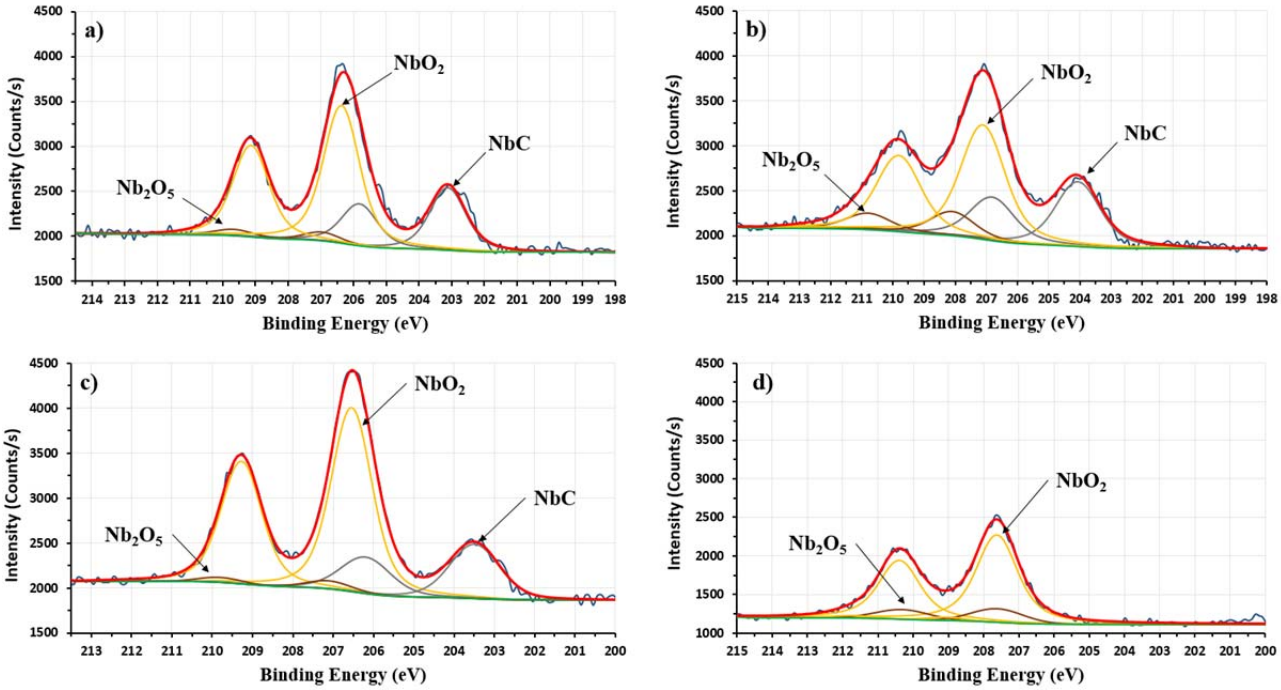

Figure 9 Niobium XPS spectra for: (a) AGA; (b) NGA; (c) PA; (d) WA IN625 powders.

3.3 Microstructure of as-HIPped IN625

3.3.1. As-HIPped Microstructure

Although all the four HIPped IN625 powders showed a fully dense microstructure, however, some differences can be found in terms of microstructural features in these four HIPped powders. The first difference is the presence of particles fraction and size at the PPBs, which is strongly dependent on the powder atomisation route. The presence of PPBs was directly linked to the previously indicated O levels in the powders, (Figure 10).

AGA showed a microstructure with a higher density of twin boundaries. It has a smaller fraction of carbides, and some PPBs can be observed. The SEM micrograph of HIPped NGA powder shows a continuous network of precipitates along the PPBs, with a stronger presence of oxycarbonitrides. These precipitates were chromium oxide (Cr_2O_3), silicon dioxide (SiO_2) (for NGA and WA) and (Mo, Nb) carbides, nitrides [24]. The particles along the PPBs were mainly Cr_2O_3, while the others, such as (Mo, Nb)C, precipitate with even distribution in the microstructure.

EDS analysis was conducted on the HIPped NGA sample (Figure 11), which shows that Cr_2O_3 acts as nucleation site for some of the carbides and nitrides.

PA HIPped microstructure has the lowest O level, and, consequently, the least amount of PPBs, with the presence of only a few small carbides. PA HIPped microstructure seems to be characterised by a bi-modal grain structure with coarse grains surrounded by finer ones; this might be attributed to the bi-modal size distribution of PA powders. Lastly, the microstructure of WA HIPped powder represents the influence of the powder's O content on the as-HIPped microstructure. In this case, all the powders are surrounded by a continuous layer of Cr_2O_3, acting as a precipitation site for some (Mo, Nb)C. Compared to NGA, the microstructure does not show any uniform precipitation of carbides, which are distributed at PPBs. This might be attributed to the lower amount of C present in WA powders. Some SEM micrographs, performed in the proximity of the steel canister, where C diffusion from the canister is likely, show a uniform distribution of carbides in the microstructure (Figure 12). This suggests that carbide formation in the early stages is driven by the presence of chromium oxides, until it reaches a saturation point. At that stage, carbides start to form uniformly within the microstructure. This assumption might sound incorrect if the microstructures of PA and AGA are observed, however, in this case, the chromium oxide should not drive the carbide formation mechanism, since both materials have a lower O content.

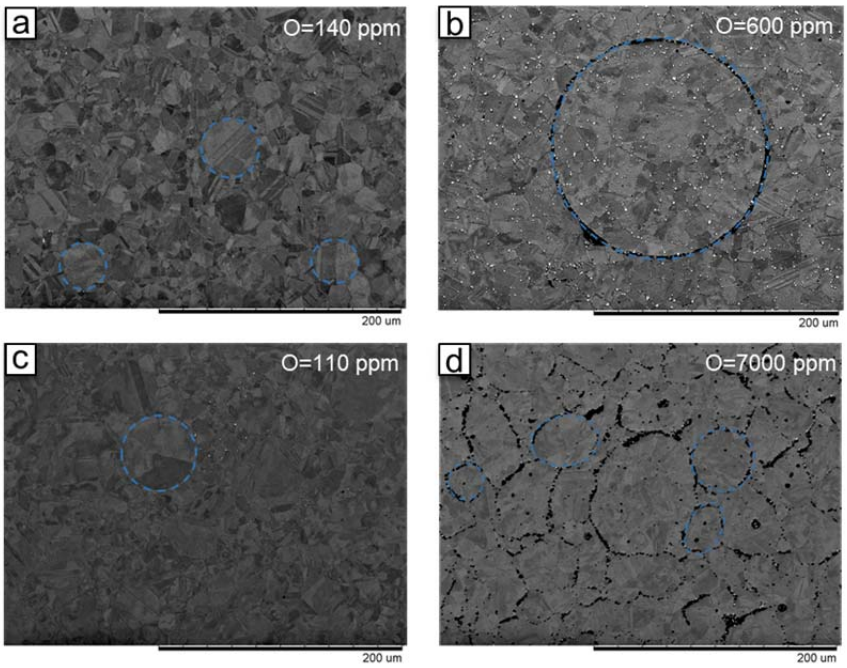

Figure 10 As-HIPped microstructure of (a) AGA; (b) NGA; (c) PA; (d) WA (PPBs highlighted in blue).

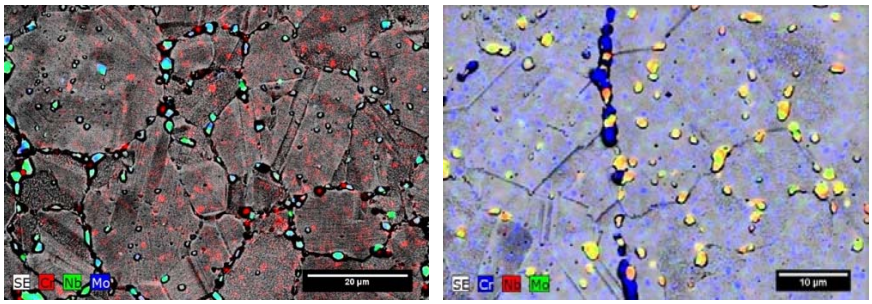

Figure 11 EDS analysis at PPBs for HIPped NGA IN625.

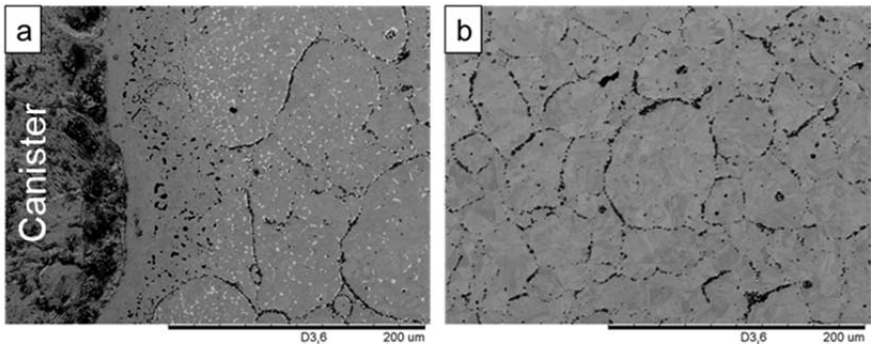

Figure 12 Carbide formation mechanism differences in HIPped WA: a) Precipitation in the proximity of the canister, showing a uniform distribution of carbide precipitation; b) precipitation far from the canister, showing carbide precipitation just at PPBs.

SEM backscattered images were used to give a first assessment on the differences between the four HIPped powder materials. However, a more detailed assessment was required to

understand the grain structure. To achieve this, EBSD analysis was performed on the AGA, NGA and PA HIPped powders. All three HIPped materials displayed a randomly oriented microstructure with equiaxed grains; a typical microstructure of HIPped material [34].

Figure 13 shows the differences within the microstructures; AGA and NGA had a similar average grain size, 10 and 13µm, respectively, while PA HIPped microstructure displayed a bi-modal distribution with coarse and fine grains with an average size of 19µm. The reason for the presence of coarse grains in PA HIPped microstructure can be attributed to the presence of bigger cell size in PA atomised powder, which is a direct consequence of the lower cooling rate of PA process. Furthermore, due to the high packing density of PA powder, lower plastic deformation occurs during the densification process, thus the stored energy in the material is lower, leading to an inhomogeneous recrystallisation in the material, and, consequently, a bi-modal grain size distribution [34]. Table 3 shows the influence of the powder atomisation route on the presence of Σ3 boundaries. AGA shows the lowest presence of Σ3 coincident site lattices (CSL) fraction (22.2%), while PA and NGA HIPped microstructure show much higher levels, respectively 42.7% and 48%. The high presence of low energy Σ3 CSL can have a beneficial impact on strain-to-failure, hydrogen embrittlement and on stress corrosion cracking, as reported in different studies [35], [36], [37].

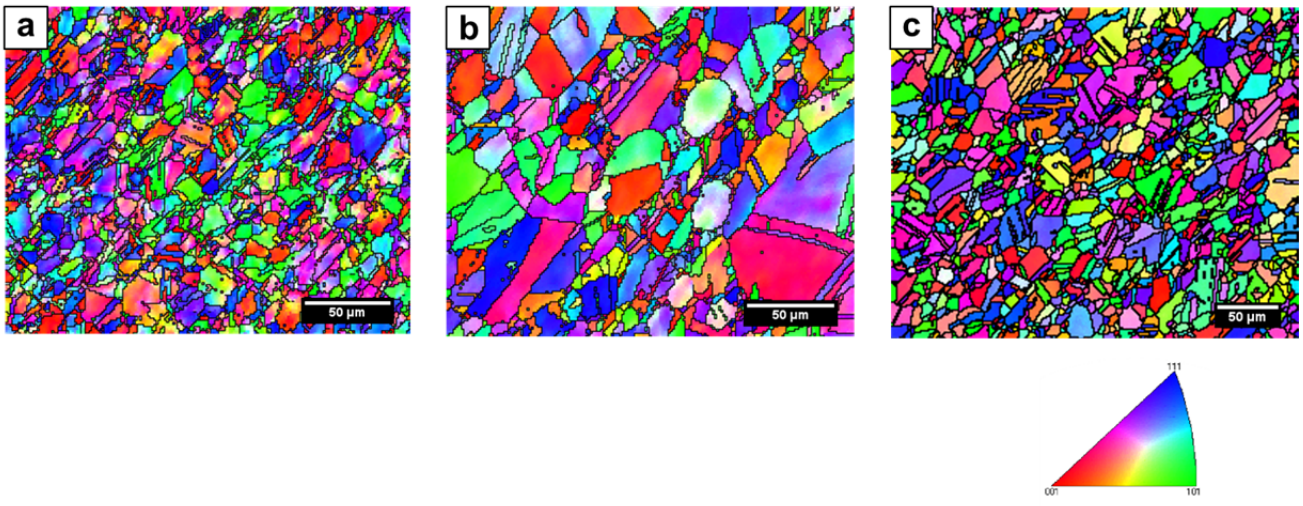

Figure 13 Inverse Pole Figures (IPF) of HIPped showing the grain structure in; (a) AGA, (b) NGA, (c) PA.

Table 3 Σ3 CSL fraction for HIPed AGA, NGA and PA IN625

HIPed Powder Type	Σ3 CSL Fraction (%)
AGA IN625	22.2
PA IN625	42.7
NGA IN625	48.0

3.3.2 Post-HIP heat treatments

After HT1, described in the experimental procedure, the four samples were analysed to understand the differences between the HIPped and heat treated (HTed) microstructure. The backscattered SEM micrographs of the samples can be seen in Figure 14. AGA had the highest amount of thermally-induced porosity (TIP), which was likely due to the entrapped argon gas porosity manifested during the argon gas atomisation process. Furthermore, NGA, PA and WA also showed some TIP (circled white in Figure 14) as well, suggesting that the SHT at temperatures of 1180°C which is higher than HIP temperature of 1160°C, provided enough driving force for the generation of TIP, irrespective of the IN625 powder atomisation type used. The presence of the undesirable phases in the HIPped and HTed IN625 powders indicated that even a high SHT temperature (1180°C), above the Laves dissolution temperature in the order of 1100°C [19], was unable to dissolve or completely eliminate the presence of oxycarbonitrides in NGA and oxides in WA from the microstructure.

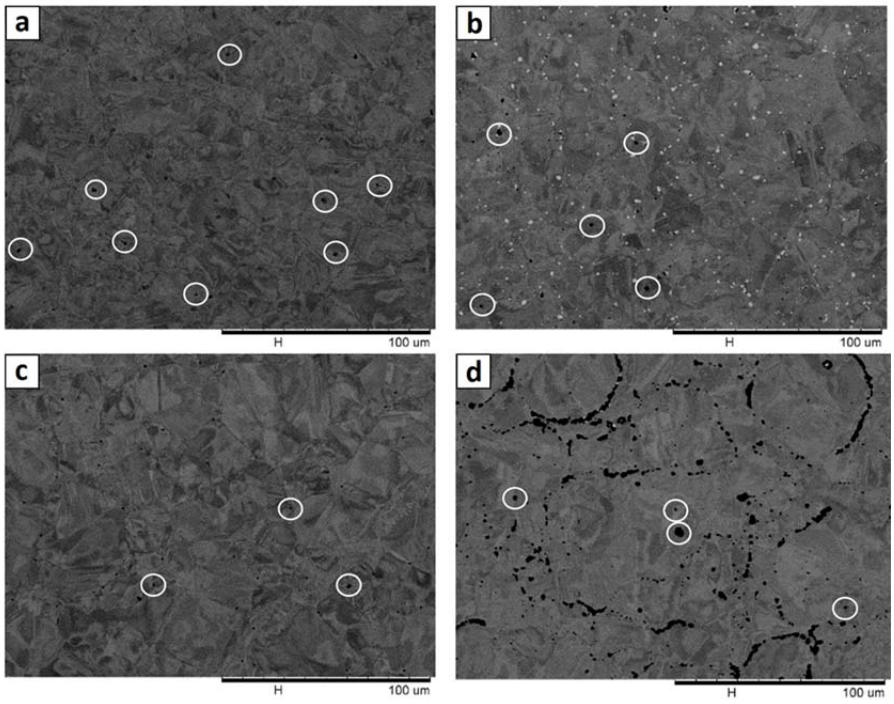

Figure 14 Backscattered SEM images of HIPped + HTed samples: (a) AGA; (b) NGA; (c) PA; (d) WA.

Another HT, called HT2 was designed with a lower SHT temperature to avoid the formation of TIP in the HIPped and HTed IN625 material [12]. It was performed on PA IN625 only, which showed the lowest amount of TIP and any undesirable phases.

The lower SHT's temperature (1050°C) aimed to avoid TIP as well as any unnecessary grain growth during the post-HIP HT process. As expected, the microstructure of HTed PA IN625 during HT2 with this new SHT strategy displayed negligible amount of TIP compared to the samples heat treated with HT1 condition (Figure 15).

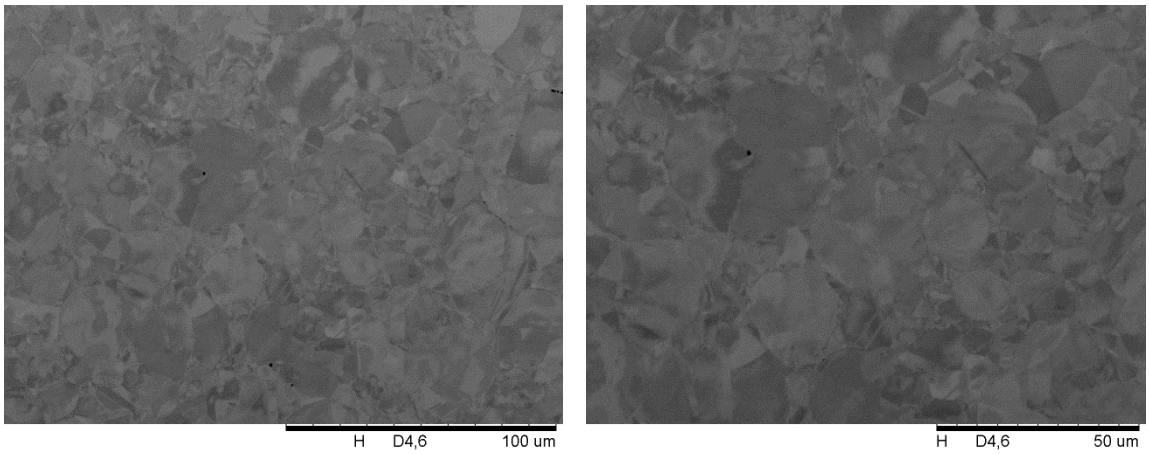

Figure 15 SEM backscattered micrographs of HIPped + HTed PA IN625 using HT2 cycle.

3.4. Mechanical properties

3.4.1. Microhardness

Microhardness tests were performed on the four HIPped and HIPped + HTed samples to understand whether the HT parameters were adequate to precipitate some amount of γ′′(Ni_3Nb) strengthening phase. Figure 16 shows the hardness of HIPped + HTed material was higher than as-HIPped material, suggesting the HT successfully precipitated some γ′′ hardening phase. A slightly higher hardness in HIPped + HTed AGA was likely due to better HT responses, thanks to the fine powder size ranges, i.e. 15-45µm, and the alloy chemistry, as some elements, such as Nb, Mo, Fe, Ti and Al, were higher when compared to other powders, especially NGA and WA (Table 1). The higher amount of Nb in AGA can give raise to the precipitation of *γ′′*, while the presence of higher levels of Mo reduced the solid solubility of reactive elements, such as Nb, Ti and Al, encouraging the precipitation hardening of the alloy [38]. As-HIPped NGA has slightly higher values of hardness, likely related to the higher fraction of oxycarbonitrides precipitation. As-HIPed PA displayed the highest standard deviation in microhardness among the four powders, this can be attributed to its bi-modal grain size distribution.

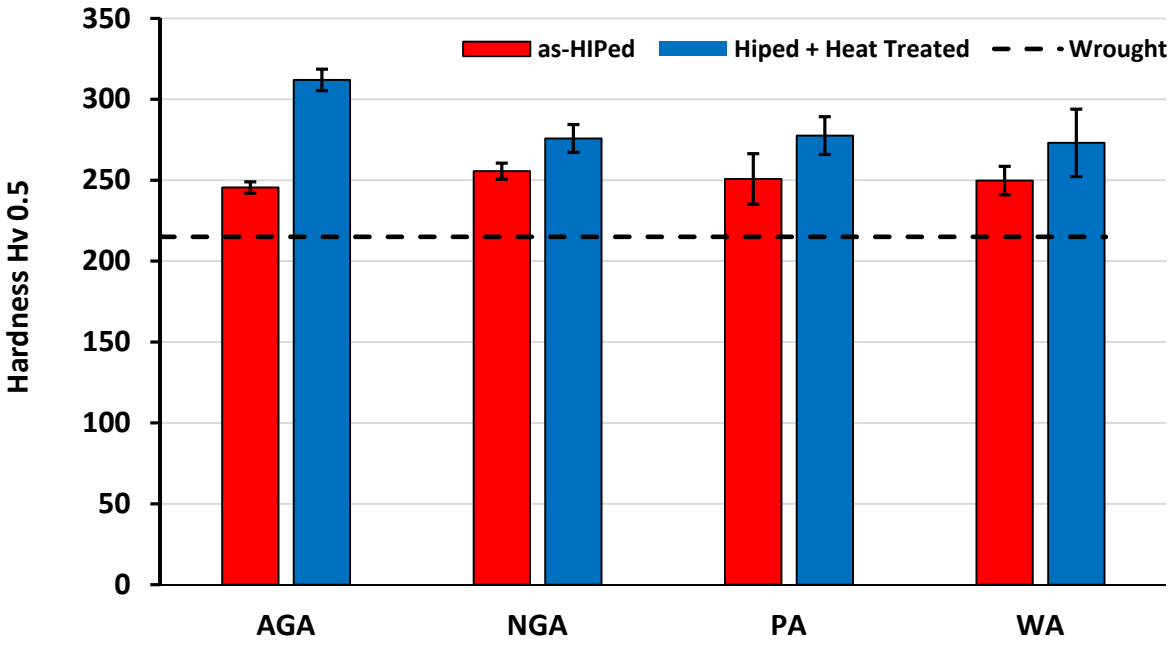

Figure 16 Microhardness of as-HIPped and HIPped + HTed AGA, NGA, PA and WA IN625.

Microhardness results were higher than wrought IN625 in as-rolled (215HV) and solution treated (160HV) conditions [40], however, tensile and fracture test data are required to better understand the as-HIPped and HIPped + HTed material properties. These tests should provide an understanding on the influence of the microstructure, especially the amount of PPBs, on properties such as yield strength (YS), ultimate tensile strength (UTS), elongation (El%) and Charpy impact energy.

3.4.2. As-HIPped tensile properties

The room temperature tensile results, shown in Figure 17, highlight how HIPped AGA has the highest YS compared to the other HIPped powders. Due to the difference in powder atomisation route and in chemistry among the four powders there are several variables influencing the yield strength. However, for AGA the presence of a finer microstructure and the relatively higher amount of Mo, Fe and Nb, providing solid solution strengthening, are certainly beneficial for improving the

YS (Table 4) [41]. Furthermore, the combined composition of O, N and C in the different batches is the least in AGA powder, meaning that low quantities of the solid solution strengthening elements are consumed in the formation of oxy-carbides or nitrides, which is when combined with the finer grain size, together result in a relatively higher YS in AGA than the other batches. All four different HIPped powders have a higher YS compared to the minimum specification for as-rolled IN625 [40]. If compared to the work of Dugdale *et al.*, where the as-HIPed IN625 was subjected to similar HIP parameters and with a post-HIP heat treatment at 900°C, AGA, NGA and PA have higher values of YS and UTS, while just PA has better elongation if compared to the aforementioned work (Figure 17) [17]. AGA, NGA and PA have similar values of UTS; however, WA has a drop in strength compared to the other powders. Furthermore, a big change in the El% behaviour can be observed from the tensile tests. As expected, the El% of WA is quite poor; AGA and NGA have similar values of El%, matching the minimum specification for wrought IN625, while PA has an El% above 40%, higher than the other three powders. The elongation can be directly linked with the O content and the amount of micro-segregated elements present on powder surface, and, consequently, the amount of PPBs present in the HIPped material, as showed in previous works [3]. PA, which has the lowest amount of O, much cleaner powder surface with minimal micro-segregated elements and PPBs, possesses the highest El%, much higher compare to AGA and NGA.

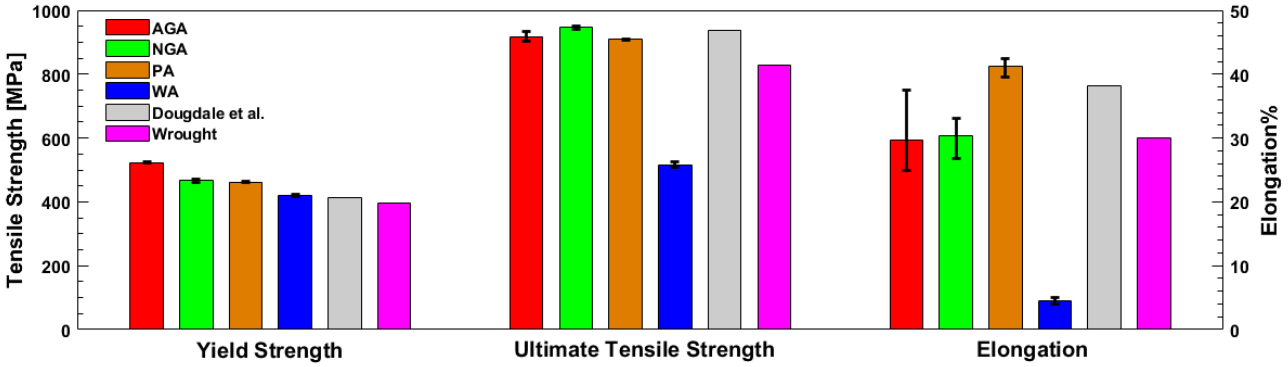

Figure 17 Room temperature tensile properties of as-HIPped IN625.

Table 4 Influence of grain size and powder chemistry on the YS of the as-HIPed IN625.

HIPed Powder	YS	Grain Size	Cr	Nb	Mo	Fe	O	C	N

Type	(MPa)	(µm)	(wt%)	(wt%)	(wt%)	(wt%)	(wt%)	(wt%)	(wt%)
AGA IN625	522	10	20.80	3.64	9.10	4.20	0.01	0.02	0.009
NGA IN625	467	13	20.32	3.18	8.48	3.12	0.06	0.009	0.07
PA IN625	462	19	21.47	3.59	8.71	1.37	0.01	0.03	0.009

To prove the influence of PPBs on the mechanical properties, fractographic analysis was performed on the fracture surface of tensile tested sample. From Figure 18**Error! Reference source not found.**, it is quite evident to affirm that for all the tensile samples, the dominating fracture mode is inter-particle fracture. However, there are some differences in the fracture surfaces. NGA and WA showed a consistent amount of oxides, carbides and oxycarbides, though with some dimples, meaning that some ductile fracture has happened. Carbides and nitrides are uniformly distributed around the particle boundaries of NGA fracture surfaces, while in WA there is more presence of Cr_2O_3 due to the high O content combined with the presence of Cr micro-segregation on the surface of the powders. These precipitates are difficult to see on the surface of PA or AGA powders, although the fracture starts on the particle boundaries. Smaller size carbides and oxides are responsible for this fracture behaviour; however, their size is small, thus making them difficult to be seen using a conventional SEM.

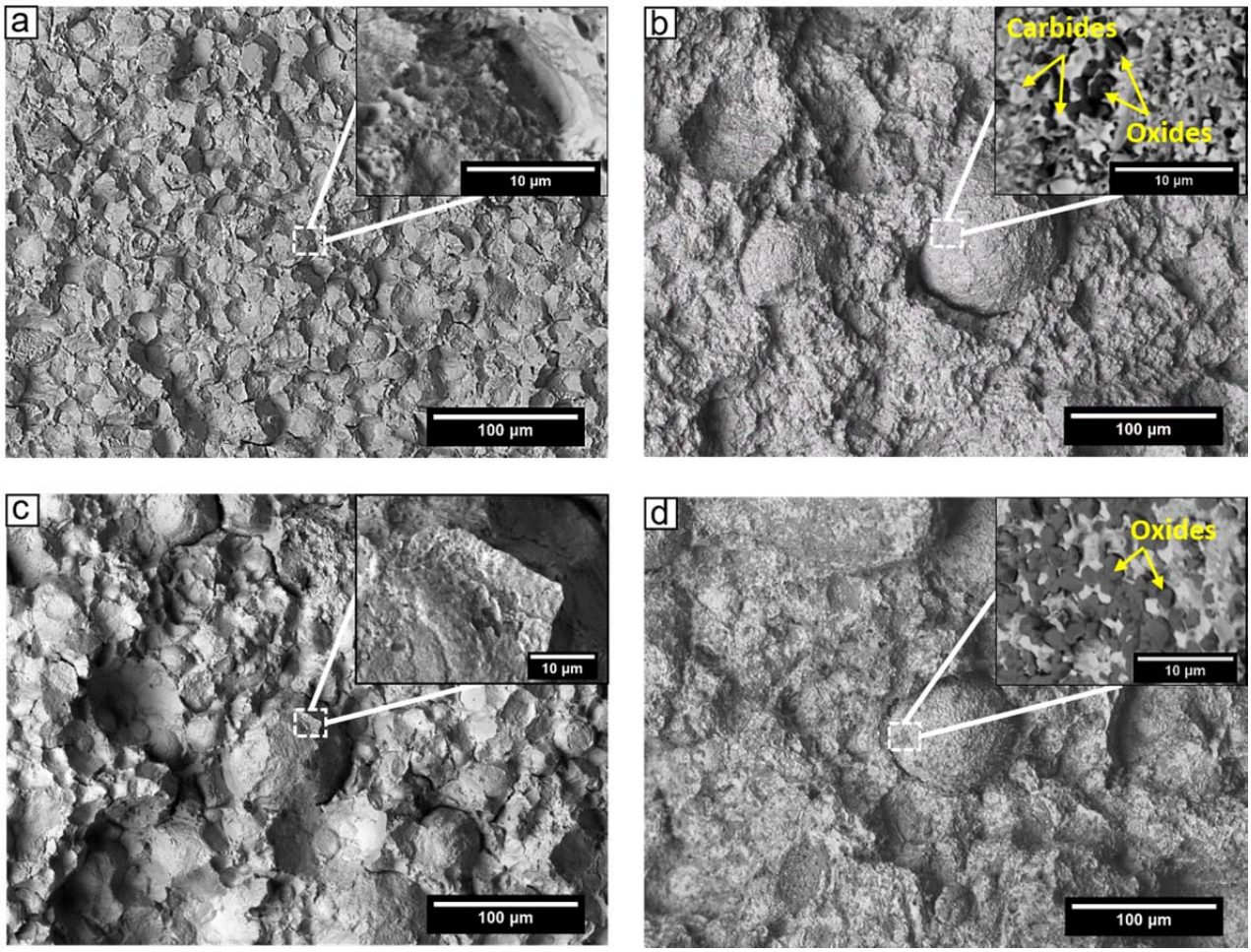

Figure 18 Fractographic analysis on as-HIPped IN625 tensile samples; (a) AGA, (b) NGA, (c) PA, (d) WA.

3.4.3. HIPped + HTed tensile properties

After HT2, PA IN625 samples were tensile tested at room temperature to understand whether the HT has any beneficial effect or not on the mechanical properties of the HIPped PA powder material. The results show similar mechanical properties with no obvious increase in strength for the HIPped + HTed condition, meaning the HT aging cycle did not precipitate enough hardening γ″ phase (Figure 19). However, there is an improvement in the El% of the material, meaning the solution of HT had a beneficial effect on making the grains grow past PPBs [12].

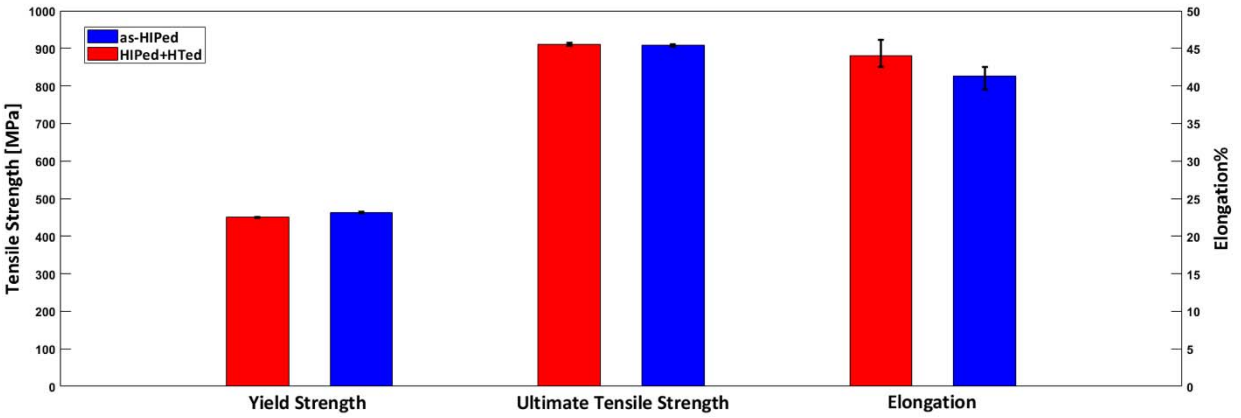

Figure 19 Room temperature tensile properties of as-HIPped PA vs HIPped + HTed PA IN625.

3.4.4. Charpy impact test

The results of the Charpy impact test (Figure 20) show that PA has the highest absorbed energy, with an average value of around 64J; close to the average value of 66J for wrought IN625 [40]. However, the absorbed energy values are lower if compared with the work of Berglund *et al.* reporting an absorbed energy ranging from 59-93J [42] and the work from Dougdale *et al.* with a Charpy absorbed energy ranging from 84-119J [17]. The lower levels of absorbed energy can be attributed to a difference in powder chemistry as highlighted by Berglund *et al.*, where a minimal difference in powder chemistry led to a considerable scatter in the absorbed energy [42]. This highlights a clear difference between AGA and NGA, which was not seen in the tensile test data results of Figure 17. WA powders have lower values of absorbed energy due to the large amount of oxides along with micro-segregated elements present on the powder surface which cannot be dissolved during any post-HIP heat treatment and act as brittle crack initiation sites during Charpy impact test.

Fractographic analysis was carried out on the fractured Charpy samples (Figure 21). The micrographs confirmed the presence of inter-particle fractures in all the different HIPped samples, and that oxycarbonitrides are responsible for the lower absorbed energy in HIPped NGA IN625. To confirm that, EDS analysis was performed on the fractured surfaces of NGA HIPped powders. The

EDS map of Figure 22 shows the presence of Cr_2O_3 and (Nb, Mo)C,N evenly distributed on the surface of the HIPped NGA powders.

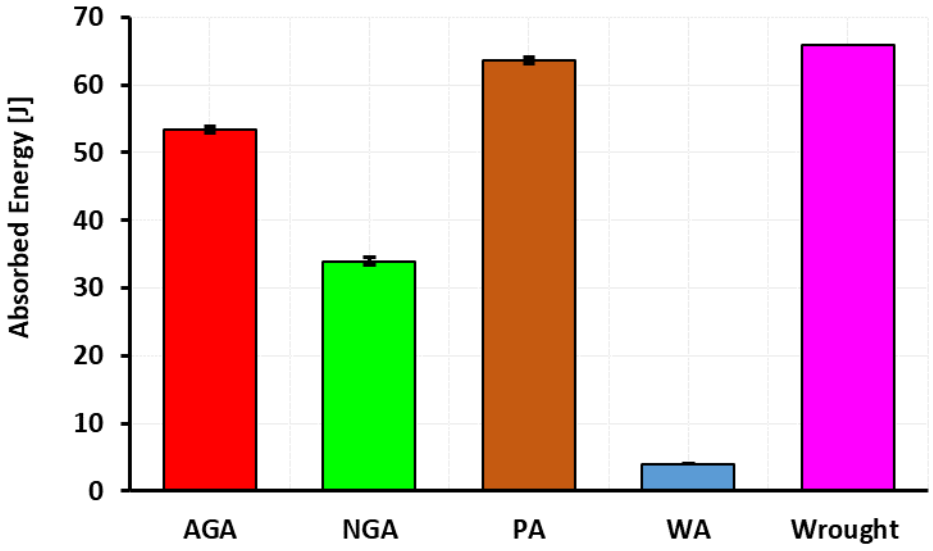

Figure 20 Charpy impact properties of as-HIPped vs wrought IN625 [40].

Figure 21 Charpy fractographic analysis of: (a) AGA, (b) NGA, (c) PA as-HIPped IN625.

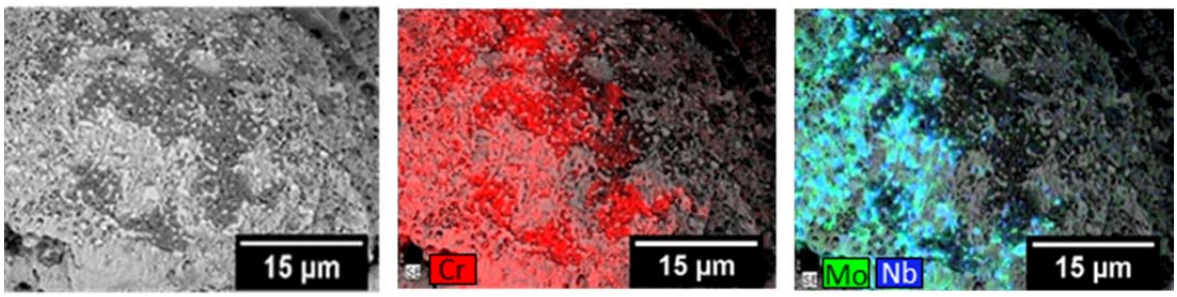

Figure 22 EDS maps for the fracture surface of NGA Charpy sample.

Charpy impact tests have also been performed on the HIPped + HTed PA. The results show that the HT had a moderate positive effect on improving the room temperature properties of HIPped IN625.

Table 5 Charpy impact properties of as-HIPped vs HIPped + HTed PA IN625.

Conditions	Absorbed Energy [J]	Std Deviation
As-HIPped PA	64.0	0.47
HIPped + HTed PA	65.6	0.45
Wrought [40]	66.0	0.00

4. Conclusions

In this study, HIPped IN625 material was developed which can be used to fabricate high value engineering parts using NNS PM HIP manufacturing technique. The main objective of this work was to understand the influence of powder atomisation route and powder characteristics on the HIPped IN625 microstructural and the mechanical properties. A detailed powder characterisation displayed a difference in morphology, packing density and in the chemistry among the four powders. XPS results showed higher concentration of O and C on the surface and micro-segregation of Cr, Nb, and Si, having a considerably detrimental effect on the formation of oxides, carbides and oxycarbides at the PPBs. The microstructure analysis shows a close relation between O level and presence of precipitates at PPBs. Those precipitates play a crucial role on material's ductility and Charpy impact absorbed energy. The analysis on WA HIPped microstructure, in the proximity of the canister as well as far from it, has confirmed that the generation oxides act as preferential precipitation sites for carbides up to a saturation point. PA HIPped powder had the best balance between tensile strength, El% and Charpy impact absorbed energy. HT performed on the four as-HIPped samples, using a SHT temperature of 1180°C, displayed a considerable presence of TIP, especially in AGA, while lowering the SHT temperature to 1050°C reduced the amount of TIP with no unnecessary grain growth in PA HIPped samples. Lastly, the second HT i.e., HT2 performed on

PA IN625 slightly improved the ductility and impact toughness properties of the material, with no adverse effect on its strength.

The main outcome of this study is that prior to considering metal powders HIPping on a specific material, its powder characteristics needs to be fully understood. A detailed chemical composition analysis is needed, especially for the powder material with elements who are strong oxide formers, such as Cr, Al, Hf or Ti etc. By selecting Ni-base superalloys powder with low amount of interstitials will allow to use HIP technology for manufacturing high value engineering parts.

Acknowledgments:

AS acknowledges the Centre of Doctoral Training in Innovative Metal Processing (IMPaCT), funded by the Engineering and Physical Sciences Research Council (EPSRC), and the National Structural Integrity Research Centre (NSIRC) for funding his PhD at the University of Birmingham. The authors warmly thank the European Union H2020 and the "Sustainable Process Industry through Resource and Energy Efficiency" (SPIRE) programmes, which funded this project under grant agreement n° 768612. The authors also acknowledge the support of the Henry Royce Institute for A. Sergi through the Royce PhD Equipment Access Scheme, enabling access to XPS at Royce@Imperial; EPSRC Grant number EP/R00661X/1.

Declarations of interest: none

Data Availability:

The raw/processed data required to reproduce these findings cannot be shared at this time due to time limitations. The authors are glad to make the data available upon request by emailing the corresponding author.

References

[1] H. V. Atkinson and S.Davies, "Fundamental aspects of hot isostatic pressing : An overview," *Metall. Mater. Trans. A*, vol. 31, pp. 2981–3000, 2000.

[2] Y. L. Kuo and K. Kakehi, "Effect of the prior particle boundary on the microstructure and mechanical

properties of hot-isostatic-pressed IN718 Alloy," *Mater. Trans.*, vol. 58, no. 7, pp. 1042–1048, 2017.

[3] G. A. Rao, M. Srinivas, and D. S. Sarma, "Effect of oxygen content of powder on microstructure and mechanical properties of hot isostatically pressed superalloy Inconel 718," *Mater. Sci. Eng. A*, vol. 435–436, pp. 84–99, 2006.

[4] Y. Hedberg, M. Norell, J. Hedberg, P. Szakálos, P. Linhardt, and I. Odnevall Wallinder, "Surface characterisation of fine inert gas and water atomised stainless steel 316L powders: Formation of thermodynamically unstable surface oxide phases," *Powder Metall.*, vol. 56, no. 2, pp. 158–163, 2013.

[5] J. Yan, Y. Zhou, R. Gu, X. Zhang, W. M. Quach, and M. Yan, "A comprehensive study of steel powders (316L, H13, P20 and 18Ni300) for their selective laser melting additive manufacturing," *Metals (Basel).*, vol. 9, no. 1, 2019.

[6] E. Gil, J. Cortés, I. Iturriza, and N. Ordás, "XPS and SEM analysis of the surface of gas atomized powder precursor of ODS ferritic steels obtained through the STARS route," *Appl. Surf. Sci.*, vol. 427, pp. 182–191, 2018.

[7] D. Chasoglou, E. Hryha, M. Norell, and L. Nyborg, "Characterization of surface oxides on water-atomized steel powder by XPS/AES depth profiling and nano-scale lateral surface analysis," *Appl. Surf. Sci.*, vol. 268, pp. 496–506, 2013.

[8] Z. J. Gao, G. Q. Zhang, Z. Li, H. Yuan, W. Y. Xu, and Y. Zhang, "Surface Segregation and Oxidation Behavior of Superalloy Powders Fabricated by Argon Atomization," *Mater. Sci. Forum*, vol. 747–748, pp. 518–525, 2013.

[9] W. Bin Ma, G. Q. Liu, B. F. Hu, P. H. Hu, and Y. W. Zhang, "Study of metallic carbide (MC) in a Ni-Co-Cr-based powder metallurgy superalloy," *Metall. Mater. Trans. A Phys. Metall. Mater. Sci.*, vol. 45, no. 1, pp. 208–217, 2014.

[10] Q. Bai, J. Lin, G. Tian, J. Zou, and D. Ta, "Review and Analysis of Powder Prior Boundary (PPB) Formation in Powder Metallurgy Processes for Nickel-based Super Alloys," *Powder Metall. Min.*, vol. 4, no. 1, pp. 1–6, 2015.

[11] L. Chang, W. Sun, Y. Cui, and R. Yang, "Influences of hot-isostatic-pressing temperature on microstructure, tensile properties and tensile fracture mode of Inconel 718 powder compact," *Mater. Sci. Eng. A*, vol. 599, pp. 186–195, 2014.

[12] J. E. Macdonald, R. H. U. Khan, M. Aristizabal, M. J. Lunt, and M. M. Attallah, "Influence of powder particle size distribution on the microstructure and mechanical properties of a HIPped CM247LC Ni superalloy," *Mater. Des.*, vol. 174, no. C, 2019.

[13] R. H. U. Khan, M. H. Loretto, M. M. Attallah, J. Cortes, I. Iturriza, and F. Castro, "Microstructure and properties of HIPped alloy 718," in *The 11th International Conference of Hot Isostatic Pressing*, 2014.

[14] John R. Dean, *Practical Inductively Coupled Plasma Spectroscopy*. Wiley, 2005.

[15] LECO, "Carbon and Sulfur Determination, LECO Induction Furnace Instruments." 2007.

[16] LECO, "Oxygen and Nitrogen Determination, LECO Inert Gas Fusion Instruments." 2007.

[17] H. R. Dugdale and J. B. Borradaile, "Development of hot isostatically pressed nickel based alloys for nuclear applications," *Powder Metall.*, vol. 56, pp. 374–381, 2013.

[18] "Heat Treatment Wrought Nickel Alloy and Cobalt Alloy Parts, in AMS 2774E. SAE International." .

[19] S. Floreen, G. E. Fuchs, and W. J. Yang, "The Metallurgy of Alloy 625," *Superalloys 718, 625, 706*

Var. Deriv., pp. 13–37, 1994.

[20] M. Sundararaman, P. Mukhopadhyay, and S. Banerjee, "Precipitation of the δ-Ni3Nb phase in two nickel base superalloys," *Metall. Trans. A*, vol. 19, no. 3, pp. 453–465, 1988.

[21] Z. Tian, C. Zhang, D. Wang, W. Liu, and X. Fang, "A Review on Laser Powder Bed Fusion of Inconel 625 Nickel-Based Alloy," *Appl. Sci.*, vol. 10, pp. 1–14, 2019.

[22] F. Xu, Y. Lv, Y. Liu, B. Xu, and P. He, "Effect of heat treatment on microstructure and mechanical properties of inconel 625 alloy fabricated by pulsed plasma arc deposition," *Phys. Procedia*, vol. 50, no. October 2012, pp. 48–54, 2013.

[23] "ASTM International. B834-17 Standard Specification for Pressure Consolidated Powder Metallurgy Iron-Nickel-Chromium-Molybdenum (UNS N08367), Nickel-Chromium-Molybdenum-Columbium (Nb) (UNS N06625), Nickel-Chromium-Iron Alloys (UNS N06600 and N06690), and N." .

[24] J. W. Wang, Q. S. Wei, G. C. Liu, Y. K. He, and Y. S. Shi, "Study on direct hot isostatic pressing technology for superalloy inconel 625," *Adv. Mater. Res.*, vol. 189–193, pp. 2935–2938, 2011.

[25] "Nickel Alloy, Corrosion and Heat-Resistant, Powder for Additive Manufacturing, 62Ni-21.5Cr-9.0Mo-3.65Nb, in AMS7001. SAE International."

[26] A. Mostafaei, E. T. Hughes, C. Hilla, E. L. Stevens, and M. Chmielus, "Data on the densification during sintering of binder jet printed samples made from water- and gas-atomized alloy 625 powders," *Data Br.*, vol. 10, pp. 116–121, 2017.

[27] O. D. Neikov, "Atomization and granulation," *Handb. Non-Ferrous Met. Powders*, pp. 102–142, 2009.

[28] F. Pengjun, X. Yi, L. Xinggang, and C. Ya, "Influence of Atomizing Gas and Cooling Rate on Solidification Characterization of Nickel-based Superalloy Powders," *Rare Met. Mater. Eng.*, vol. 47, no. 2, pp. 423–430, 2018.

[29] C. Pleass and S. Jothi, "Influence of powder characteristics and additive manufacturing process parameters on the microstructure and mechanical behaviour of Inconel 625 fabricated by Selective Laser Melting," *Addit. Manuf.*, vol. 24, no. September, pp. 419–431, 2018.

[30] S. D. DuPont, John N. Lippold, John C. Kiser, *WELDING METALLURGY AND WELDABILITY OF NICKEL-BASE ALLOYS*. John Wiley & Sons, Inc, 2009.

[31] F. J. Rizzo and D. J. Radavich, "Microstructural Characterization of PM 625-Type Materials," in *Superalloys 718,625 and Various Derivatives*, 1991, pp. 297–308.

[32] A. Gupta, M. Mittal, M. K. Singh, S. L. Suib, and O. P. Pandey, "Low temperature synthesis of NbC/C nano-composites as visible light photoactive catalyst," *Sci. Rep.*, vol. 8, no. 1, pp. 1–17, 2018.

[33] F. J. Rizzo, "Strengthening Precipitates in Argon Atomized PM 625," *TMS*, pp. 913–922, 1994.

[34] S. Irukuvarghula, H. Hassanin, C. Cayron, M. Aristizabal, M. M. Attallah, and M. Preuss, "Effect of powder characteristics and oxygen content on modifications to the microstructural topology during hot isostatic pressing of an austenitic steel," *Acta Mater.*, 2019.

[35] V. Randle, M. Coleman, and G. Owen, "Evolution of the Grain Boundary Network as a Consequence of Deformation and Annealing," *Mater. Sci. Forum*, vol. 550, pp. 35–44, 2007.

[36] M. Detrois and R. Goetz, "Grain boundary engineering of powder processed Ni-base superalloy RR1000 : Influence of the deformation parameters," *Mater. Sci. Eng. A*, vol. 627, pp. 95–105, 2015.

[37] S. Bechtle, M. Kumar, B. P. Somerday, M. E. Launey, and R. O. Ritchie, "Grain-boundary

engineering markedly reduces susceptibility to intergranular hydrogen embrittlement in metallic materials," *Acta Mater.*, vol. 57, no. 14, pp. 4148–4157, 2009.

[38] H. L. Eiselstein and D. J. Tillack, "The Invention and Definition of Alloy 625," in *Superalloys 718, 625, 716 and derivatives*, 1991, pp. 1–14.

[39] C. Wei-Di and K. Richard, "Role of Chemistry in 718-Type Alloys - Allvac 718Plus Alloy Development," in *Superalloys 2004*, 2004.

[40] S. Metals, "Inconel Alloy 625," *www.Specialmetals.com*, vol. 625, no. 2, pp. 1–28, 2013.

[41] A. J. Goodfellow, "Strengthening mechanisms in polycrystalline nickel-based superalloys," *Mater. Sci. Technol. (United Kingdom)*, vol. 34, no. 15, pp. 1793–1808, 2018.

[42] T. Berglund and F. Meurling, "Oxygen Content in PM HIP 625 and its Effect on Toughness," *12th Int. Conf. Hot Isostatic Press.*, pp. 135–141, 2017.